Uncertainties in rainfall kinetic energy-intensity relations for soil erosion modelling

Florian Wilken[a,b], Martin Baur[a], Michael Sommer[b,c], Detlef Deumlich[d], Oliver Bens[e], Peter Fiener[a,*]

[a] Institute for Geography, Universität Augsburg, Augsburg, Germany
[b] Working Group Landscape Pedology, Leibniz-Centre for Agricultural Landscape Research ZALF e.V., Müncheberg, Germany
[c] University of Potsdam, Institute of Earth and Environmental Sciences, Potsdam, Germany
[d] Working Group Hydropedology, Leibniz-Centre for Agricultural Landscape Research ZALF e.V., Müncheberg, Germany
[e] Helmholtz Centre Potsdam GFZ German Research Centre for Geosciences, Germany

ARTICLE INFO

Keywords:
Rainfall kinetic energy
Drop size distribution
Drop fall velocity
Soil erosion modelling
Optical distrometer

ABSTRACT

For bare soil conditions, the most important process driving and initiating splash and interrill erosion is the detachment of soil particles via raindrop impact. The kinetic energy of a rainfall event is controlled by the drop size and fall velocity distribution, which is often directly or indirectly implemented in erosion models. Therefore, numerous theoretical functions have been developed for the estimation of rainfall kinetic energy from available rainfall intensity measurements. The aim of this study is to assess differences inherent in a wide number of kinetic energy-rainfall intensity (KE-I) relations and their role in soil erosion modelling. Therefore, 32 *KE-I* relations are compared against measured rainfall energies based on optical distrometer measurements carried out at five stations of two substantially different rainfall regimes. These allow for continuous high-resolution (1-min) direct measurements of rainfall kinetic energies from a detailed spectrum of measured drop sizes and corresponding fall velocities. To quantify the effect of different *KE-I* relations on sediment delivery, we apply the erosion model WATEM/SEDEM in an experimental setup to four catchments of NE-Germany. The distrometer data shows substantial differences between measured and theoretical models of drop size and fall velocity distributions. For low intensities the number of small drops is overestimated by the Marshall and Palmer (1948; MP) drop size distribution, while for high intensities the proportion of large drops is overestimated by the MP distribution. The distrometer measurements show a considerable proportion of large drops falling at slower velocities than predicted by the Gunn and Kinzer (1949) terminal velocity model. For almost all rainfall events at all stations, the *KE-I* relations predicted higher cumulative kinetic energy sums compared to the direct measurements of the optical distrometers. The different *KE-I* relations show individual characteristics over the course of rainfall intensity levels. Our results indicate a high sensitivity (up to a range from 10 to 27 t ha^{-1}) of the simulated sediment delivery related to different *KE-I* relations. Hence, the uncertainty associated with *KE-I* relations for soil erosion modelling is of critical importance.

1. Introduction

Rainfall driven soil erosion is traditionally subdivided into a number of sub-processes, ranging from raindrop impact driven splash and interrill erosion to surface runoff based rill and gully erosion processes. Particularly initial soil erosion processes are closely related to the rainfall kinetic energy (*KE*) that controls soil detachment, aggregate disruption and transport by rain splash. Moreover, rain drop impact on bare soil causes soil crusting and a corresponding infiltration reduction (Morgan, 2005), and leads to turbulences in shallow surface runoff that affects the transport capacity (Kinnell, 2005). Due to these direct and indirect implications of the *KE* of raindrops on several erosion processes *KE* is widely used as an important input parameter in erosion models. It is implemented in conceptual and empirical models, especially the USLE (Wischmeier and Smith, 1960) and its derivatives (RUSLE: Renard et al., 1996; WaTEM/SEDEM: Van Oost et al., 2000) as well as in physically-oriented models (LISEM: De Roo et al., 1996; EUROSEM: Morgan et al., 1998).

The assessment of rainfall *KE* started more than a century ago with the pioneer work of Wiesner (1895) and Bentley (1904) who introduced

* Corresponding author.
E-mail address: fiener@geo.uni-augsburg.de (P. Fiener).

Table 1
Table of theoretical relationships for rainfall kinetic energy ($J\,m^{-2}\,h^{-1}$) and rainfall intensity (I: $mm\,h^{-1}$; see Fig. 1). Majority of equations are harmonized according to Salles et al. (2002).

Original reference	Equation	Region
Logartithmic		
Wischmeier and Smith, 1958	$I\,(11.9 + 8.73\,\log_{10} I)$ if $I \leq 76\,mm\,h^{-1}$ if $I > 76\,mm\,h^{-1}$; $KE = 28.3\,J\,m^{-2}\,mm^{-1}$	–
Zanchi & Torri 1980	$I\,(9.81 + 11.25\,\log_{10} I)$	Italy
Kinnell 1981[a]	$I\,(17.12 + 5.23\,\log_{10} I)$	USA (Florida)
Onaga et al. 1988	$I\,(9.81 + 10.6\,\log_{10} I)$	Japan (Okinawa)
Brandt 1990	$I\,(8.95 + 8.44\,\log_{10} I)$	–
Exponential		
McGregor & Mutchler 1976	$I\,(27.3 + 21.68\,e^{-0.048\,I} - 41.26\,e^{-0.072\,I})$	USA
Kinnell 1981[b]	$29.31\,I\,(1–0.281\,e^{-0.018\,I})$	USA (Florida)
Rosewell 1986[a]	$29\,I\,(1–0.596\,e^{-0.0404\,I})$	Australia (NSW)
Rosewell 1986[b]	$26.35\,I\,(1–0.669\,e^{-0.0349\,I})$	Australia (Queensland)
Brown & Foster 1987	$29\,I\,(1–0.72\,e^{-0.05\,I})$	USA
Coutinho & Tomás 1995	$35.9\,I\,(1–0.559\,e^{-0.034\,I})$	Portugal
Cerro et al., 1998	$38.4\,I\,(1–0.538\,e^{-0.029\,I})$	Spain
Jayawardena & Rezaur 2000	$36.8\,I\,(1–0.691\,e^{-0.038\,I})$	China (Hong Kong)
Fornis et al. 2005	$30.8\,I\,(1–0.550\,e^{-0.031\,I})$	Philippines
Intensity power		
Park et al. 1980	$21.1\,I^{1.156}$	USA
Smith & De Veaux 1992[a]	$13\,I^{1.21}$	USA (Oregon)
Smith & De Veaux 1992[b]	$11\,I^{1.23}$	USA (Alaska)
Smith & De Veaux 1992[c]	$18\,I^{1.24}$	USA (Arizona)
Smith & De Veaux 1992[d]	$11\,I^{1.17}$	USA (New Jersey)
Smith & De Veaux 1992[e]	$10\,I^{1.18}$	USA (North Carolina)
Smith & De Veaux 1992[f]	$11\,I^{1.14}$	USA (Florida)
Uijlenhoet & Stricker 1999[a]	$7.20\,I^{1.32}$	–
Uijlenhoet & Stricker 1999[b]	$8.53\,I^{1.29}$	–
Uijlenhoet & Stricker 1999[c]	$8.46\,I^{1.17}$	–
Uijlenhoet & Stricker 1999[d]	$8.89\,I^{1.28}$	–
Uijlenhoet & Stricker 1999[e]	$10.8\,I^{1.06}$	–
Uijlenhoet & Stricker 1999[f]	$7.74\,I^{1.35}$	–
Steiner & Smith 2000	$11\,I^{1.25}$	USA (Mississippi)
Shin et al. 2016	$10.3\,I^{1.22}$	–
Others		
Carter et al. 1974	$11.32\,I + 0.5546\,I^2–0.5009\,10^{-2}\,I^3 + 0.126\,10^{-4}\,I^4$	USA (south central)
Usón and Ramos, 2001	$23.4\,I–18$	Spain
Nyssen et al. 2005	$36.65\,(I–0.6/I)$	Ethiopia

the filter-paper and fleur pellet method to measure drop size distributions. Later, Laws and Parsons (1943) and Marshall and Palmer (1948) found an exponential relation between drop size distribution (*DSD*) and rainfall intensity and furthermore Laws (1941) and Gunn and Kinzer (1949) developed a model for the terminal velocity of different drop sizes used to calculate drop size specific fall velocities. Linking the models of *DSD* and terminal velocity provided the necessary information to calculate *KE* as a function of rainfall intensity. The most prominent *KE-I* relation in erosion research was published by Wischmeier and Smith (1958). The authors used a relation between *DSD* and intensity from Laws and Parsons (1943) with a combined approach of Laws (1941) and Gunn and Kinzer (1949) of drop size specific fall velocities to calculate rainfall *KE*. Based on the calculated *KE*, a regression equation between *KE* and intensity was derived and used as the basis for the first erosivity index of the Universal Soil Loss Equation (USLE; Wischmeier and Smith, 1960). Later, other combinations of *DSD* and drop size specific fall velocities were used to calculate rainfall kinetic energy, whereas the *DSD* of Marshall and Palmer (1948) is the most frequently used (Renard et al., 1997). Based on new rainfall measuring techniques that enable the continuous and simultaneous recording of drop sizes and fall velocities (e.g. optical distrometer), it was shown that drop size and fall velocity distributions can have complex patterns between different storm events (Sempere-Torres et al., 2000), and also vary during different phases within a rainfall event (Angulo-Martinez et al., 2016). To date, a few *KE-I* relations are based on continuous measurements of drop size distributions (e.g. Cerro et al., 1998; Petan et al., 2010; Sanchez-Moreno et al., 2012), but almost no *KE-I* relation is based on both continuously measured drops size and fall velocity distributions. Instead, continuous *DSD* measurements are linked to terminal velocity models (except for Lim et al., 2015). Nonetheless, recent research shows that a large amount of drops is not well represented by terminal velocity models, which might have large implications for deriving rainfall *KE* from intensity (Angulo-Martinez et al., 2016; Larsen et al., 2014; Montero-Martinez and Garcia-Garcia, 2016).

The aims of this study are (i) to analyze potential differences between measured and theoretically derived *KE* using state of the art measuring techniques to directly calculate/measure *KE* from measured drop sizes and fall velocities, (ii) to test a large number of published *KE-I* relations to understand systematic differences between measured and derived *KE-I* relations against the background of regional rainfall regimes and (iii) to use the different *KE* results as input in a water erosion and sediment transport model to quantify the 'erosion-uncertainty' associated with different *KE* approaches.

2. Materials and methods

2.1. Rainfall, drop size distribution and fall velocity data

2.1.1. Measured and derived rainfall KE

Rainfall intensity, drop size distribution and drop size specific fall velocity are available at five stations in two different regions of Germany equipped with optical laser distrometers (Laser Precipitation Monitor: Thies-Clima, Germany). The distrometers are mounted at a height of 1 m and record the full spectrum of drop size and fall velocity

distributions. Technically, the shade of a falling drop passing a flat laser beam (228 × 20 mm) is measured. The corresponding amplitude of signal reduction is used to calculate the drop diameter, whereas the duration of signal reduction determines the fall velocity of the drop (Thies-Clima, 2011). Each raindrop is measured individually and classified into 22 particle size classes ranging from 0.125 to 8 mm (largest class ranges from 8 mm to infinity) and 20 fall velocity classes ranging from < 0.2 to 20 m s^{-1}, respectively. Therefore, all the required information is available to directly calculate the rainfall *KE* (in Joule) as

$$KE = \frac{1}{2}mv^2 \quad (1)$$

where m is the drop mass (kg) and v is the fall velocity (m s^{-1}). The device corrects for the drag force induced deformation of a falling drop and returns the drop diameter that represents the drop volume. Therefore, m can be calculated as

$$m = \frac{4}{3}\pi\rho r^3 \quad (2)$$

where r is the radius in meter and water density (ρ) is assumed to be 1 Mg m^{-3}. *KE* calculated from drop size and fall velocity based on measurements of the optical distrometer are subsequently referred to as measured *KE*.

For a better mechanistic understanding of *KE-I* relations, measured *DSD* and fall velocities are compared against traditional models (fall velocity: Gunn and Kinzer, 1949; *DSD*: Marshall and Palmer, 1948). Therefore, a comparison between measured and derived *DSDs* of different rainfall intensity ranges is analysed. Furthermore, measured drop size and fall velocity distributions are assessed in terms of the counted number of drops and their corresponding kinetic energy and compared against the theoretical fall velocity model.

For comparison against the measured *KE* we used 32 published *KE-I* relations (Table 1; Fig. 1) to derive rainfall *KE* from intensity (subsequently referred to as derived *KE*). The selection of equations cover the most common *KE-I* relations representing all equation types published (linear, logarithmic, exponential and power functions; reference see Table 1). Both measured and derived *KE* are calculated based on optical distrometer measurements of the same devices. For full comparability of the measured rainfall amount, the rainfall intensity, which is the input for the *KE-I* relations, is based on the corresponding drop volume that is also used for the direct measurements of the *KE*. All *KE-I* relations are validated against the reference, which is based on measured *KE* that is directly calculated from drop size and fall velocity values.

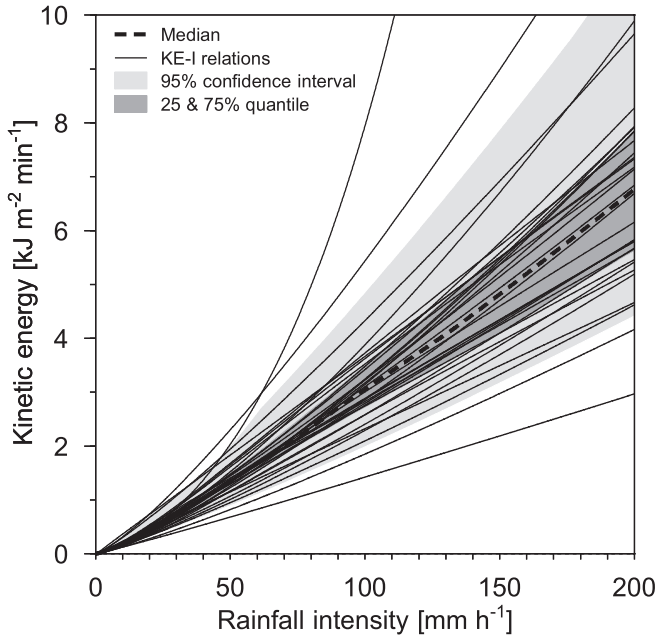

Fig. 1. Rainfall kinetic energy-intensity (*KE-I*) relations based on the equations given in Table 1.

Table 2
Descriptive statistics of observed annual rainfall data. Following Schwertmann et al. (1990), an erosive rainfall event was classified according to the exceedance of 10 mm total rainfall or 5 mm rainfall within 30 min. Individual events are separated by 6 h without observed rainfall (I_{30}: maximum 30-min rainfall intensity).

Station	Year	Sum of erosive events [mm]	No. of erosive events	Max event sum [mm]	I_{30} [mm h^{-1}]
Uck1	2015	173	15	28.2	15.4
	2016	203	12	38.0	73.7
Uck2	2015	199	15	35.8	19.6
	2016	238	12	47.7	92.5
Rur1	2015	578	20	91.5	22.3
	2016	545	16	46.6	39.9
Rur2	2013	396	19	49.0	22.5
	2015	461	16	67.0	40.9
	2016	193	10	38.9	50.1
Rur3	2013	328	19	34.9	52.1
	2014	95	6	39.1	78.1
	2015	357	21	51.3	20.5
	2016	219	12	36.2	21.6

2.1.2. Distrometer data set

The data set covers distrometer measurements made at 5 locations of 1.9 × 10^5 min during erosive events (Table 2). Two stations are located in the Uckermark in the Northeast of Germany (Fig. 2), representing a relatively dry and continental climate (mean annual precipitation 483 mm and temperature 8.7 °C; Aldana-Jague et al., 2016). The stations are mounted both in close proximity (300 m distance between stations) to the small catchments that are modelled (see Section 2.2.1). Furthermore, three stations are located in the Rur catchment in Western Germany (Fig. 2), representing a relatively wet and oceanic climate. The distances between the stations are much larger compared to the Uckermark stations (13 km minimum distance), where two stations are located in the hilly Eifel region (Rur1 and Rur2: mean annual precipitation up to 1300 mm, Graf et al., 2014, and temperature 8 °C) and the third station is located in flat and intensively used arable land close to the village of Selhausen (Rur3: mean annual precipitation 700 mm and temperature 10 °C; Reichenau et al., 2016).

For general differences between the meteorological stations in the Uckermark and the Rur region see Table 2. The heaviest precipitation event (maximum 30-min rainfall intensities: I_{30}) of the dataset occurred at the Uckermark stations in June 2016 (Uck1 I_{30}: 73.7 mm h^{-1}; Uck2 I_{30}: 92.5 mm h^{-1}; Table 2). However, the Rur stations recorded higher rainfall amounts and larger numbers of erosive rainfall events per year, whereas I_{30} are higher at the Uckermark stations.

2.2. Erosion modelling

2.2.1. Test site

The modelling test site (53°21′2 N, 13°39′5 E) consists of four small catchments (0.3 to 1.5 ha) located in the proximity of the distrometer stations in the Uckermark (Fig. 2). The study area represents a hummocky ground morainic landscape of the Weichselian glacial belt ('young morainic area') of northeastern Germany. Characteristic for these landscapes are widespread closed depressions, so-called kettle holes, which result from a delayed melting of dead ice blocks. They are nowadays filled with mineral soil, (degraded) peat or water. The four modelled TERENO observatory (Puetz et al., 2016; Zacharias et al., 2011) catchments drain into a kettle hole and consist of different sizes and slope characteristics that possesses heterogeneous sediment delivery ratios into the kettle hole. A typical conventional tillage crop

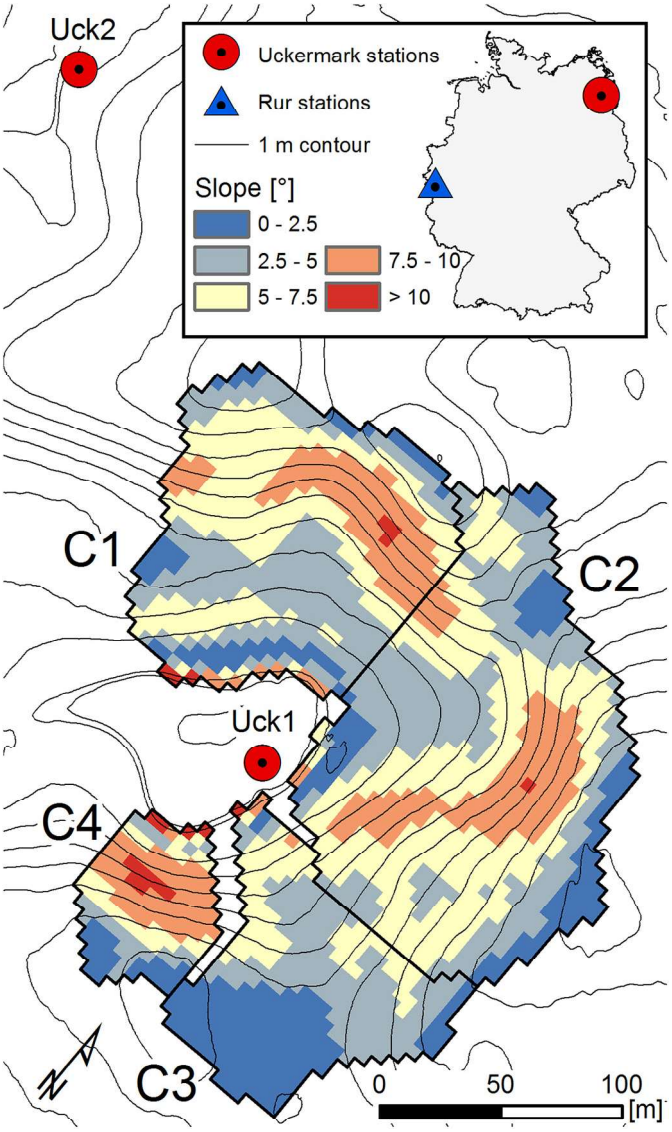

Fig. 2. Location of rainfall stations in the Uckermark and Rur region and topography of the modelled kettle hole catchments (C1–C4). (For interpretation of the references to colour in this figure legend, the reader is referred to the web version of this article.)

rotation in the Uckermark region is rape (*Brassica napus* L.) – winter wheat (*Triticum aestivum* L.) - winter barley (*Hordeum vulgare* L.), cultivated without cover crops, which is adapted for the highly fertile soils of the region. The soils are developed from glacial till and vary with respect to their location in the landscape. The soil cover of the study area reflects prolonged erosion and deposition processes due to long-term arable land use since medieval times. Only 10–15% of the area consists of soils unaffected by soil erosion (Luvisols, Stagnosols, Arenosols). Convex hilltops and steep slopes are dominated by extremely eroded A-C profiles (Calcaric Regosols, soil classification according to: IUSS, 2015). While Luvisols showing different degrees of erosion are typically situated at the up and midslopes, the footslopes and depressions show a sequence of Gleyic-Colluvic Regosols, Mollic Gleysols and (buried) Terric Histosols (Gerke et al., 2010; Sommer et al., 2008). The closed depression itself is built up by degraded Histosols and covered by a colluvial layer of mineral topsoil material (40–100 cm). Between 7 and 11 erosive rainfall events per year take place (Deumlich, 1999). In the region, maximum intensities up to 103 mm h^{-1} (per 30-min interval) were recorded during an extreme event in June 2007 (Vogel et al., 2016).

2.2.2. WaTEM/SEDEM

We utilized the water erosion module WaTEM/SEDEM (Van Oost et al., 2000; Van Rompaey et al., 2001) as implemented in the model SPEROS-C (Fiener et al., 2015; Nadeu et al., 2015; Van Oost et al., 2005). WaTEM/SEDEM is a widely used spatially explicit water erosion model, which is based on a gridded application of the Revised Universal Soil Loss Equation (RUSLE: Renard et al., 1996), which is coupled to a sediment transport and deposition approach. Where erosion is calculated according to a slightly modified RUSLE approach, transport and deposition is based on the grid cell specific local transport capacity *TC* (kg m^{-1} a^{-1}), which multiplies RUSLE factors with a transport capacity coefficient (*ktc*; in meter)

$$TC = ktc\ R\ C\ K\ L\ S\ P \tag{3}$$

where *R*, *C*, *K*, *L*, *S* and *P* are the RUSLE factors (see Renard et al., 1996): The model input rainfall-runoff erosivity (*R*) factor and cover-management (*C*) factor are directly or indirectly related to the rainfall *KE*. The annual *R* factor is calculated following Renard et al. (1996)

$$R = \sum_{i=1}^{j} (EI_{30})_i \tag{4}$$

where *E* is the rainfall *KE* of event *i* (kJ m^{-2}) and I_{30} is the maximum 30 min rainfall intensity during an event. As the product of EI_{30} is the event based rainfall erosivity. The *C* factor is calculated from daily rainfall erosivity proportions (based on 1-min *KE* values) that represent the distribution of the rainfall erosion potential over the course of the year. Subsequently, the rainfall erosivity distribution is related to the average daily soil cover of the applied crop rotation. Therefore, the *C* factor relates the intra-annual distribution of rainfall erosivity to the soil cover distribution (for more information see Renard et al., 1996). The average soil cover per day of the modelled crop rotation is based on sow and harvest dates combined with a typical crop cover development given by Schwertmann et al. (1990). The *L* factor is calculated by an approach of Desmet and Govers (1996) using the unit contributing area; the slope (*S*) factor is calculated according to McCool et al. (1987).

2.2.3. Model implementation

For the model-based analysis we used a virtual rainfall and crop rotation input data set for the four catchments. The data set combines 13 yrs. of rainfall measurements from the 5 different stations with the typical 4-year crop rotation at the test site in the Uckermark and results in 52 yrs. of independent annual rainfall-crop combinations. For these rainfall-crop combinations, the *R* and *C* factor per year were calculated for the measured *KE* and the 32 *KE-I* relations (Table 1). All other RUSLE factors where kept constant during the overall 1664 model runs to isolate the effect of different *KE-I* relations on soil erosion and sediment delivery.

According to the Federal Institute for Geosciences and Natural Resources Germany (BGR, 2014) a RUSLE *K* factor of 0.25 (Mg h) (ha N)$^{-1}$ for sandy loam was applied. The *P* factor was set to 1 as no soil conservation measures are applied at the test site. According to measurements of Gerke and Hierold (2012) at a nearby (9 km east) located study area, the topsoil bulk density was set to 1550 kg m^{-3}. Based on a study of Van Oost et al. (2003), who assessed measured *ktc* values (Verstraeten et al., 2006) against different grid sizes, a *ktc* value of 150 m was used. The model operates on a 5 × 5 m grid resolution. Topographic information is based on an airborne laser scanning digital elevation model aggregated to 5 × 5 m resolution.

3. Results

3.1. Drop size and terminal velocity distributions

Comparing the measured *DSD* of station Uck1 against the theoretical *DSD* model of Marshall and Palmer (1948; MP) indicates rainfall

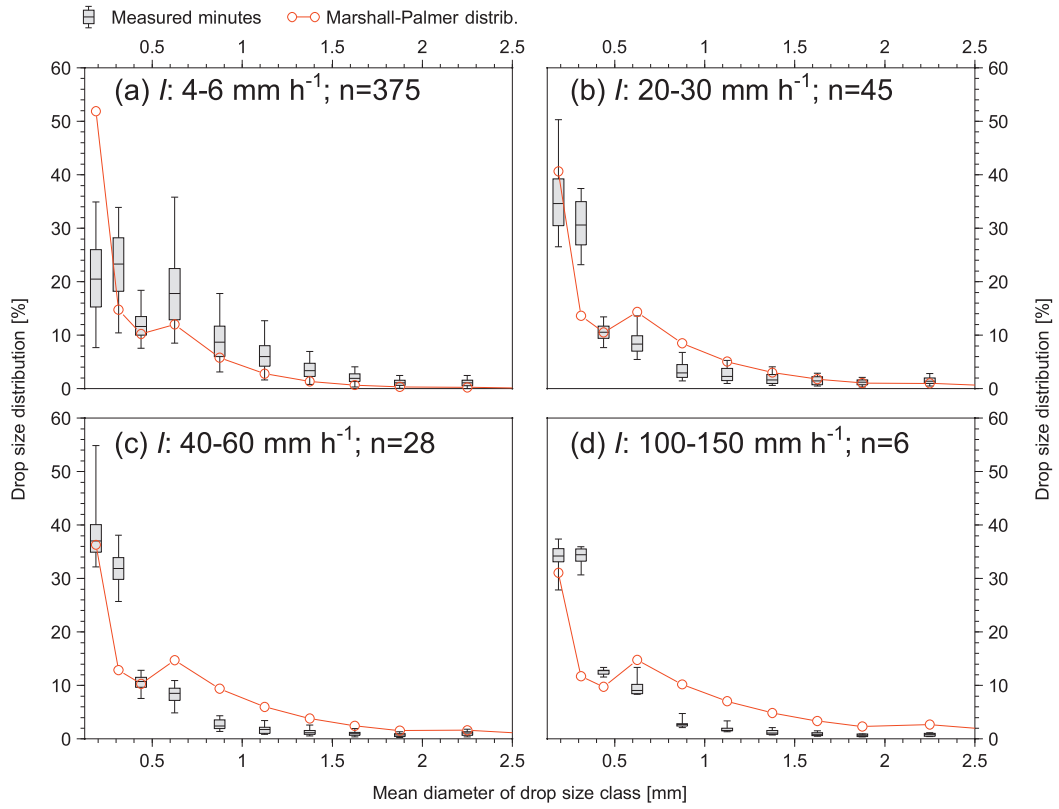

Fig. 3. Measured drop size distributions for minutes of a specific rainfall intensity range (*I*; boxes) compared to the drop size distribution model of Marshall and Palmer (1948). The variation of the Marshall-Palmer distribution for the analysed intensity ranges is small and covered by the diameter of the red marker circles. Exemplarily shown for station Uck1 (see Fig. 2). (For interpretation of the references to colour in this figure legend, the reader is referred to the web version of this article.)

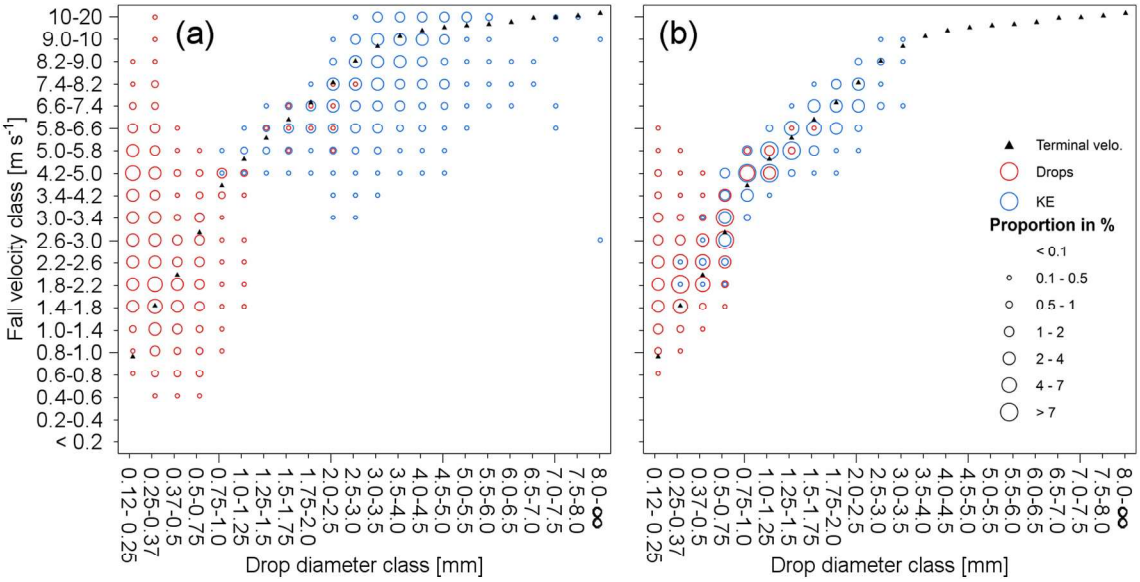

Fig. 4. Measured proportions of individual drops and rainfall kinetic energies of specific drop size and fall velocity classes. Exemplarily shown for (a) a heavy erosive rain event (sum: 38 mm; I_{10}: 162 mm h^{-1} I_{30}: 74 mm h^{-1}) and (b) a moderate erosive rain event (sum: 11 mm; I_{10}: 1.8 mm h^{-1}, I_{30}: 1.5 mm h^{-1}) at the study site Uck1 (see Fig. 2). Terminal velocity according to Gunn and Kinzer (1949) is represented in black triangles. (For interpretation of the references to colour in this figure legend, the reader is referred to the web version of this article.)

intensity specific differences (Fig. 3). (i) For minutes of low rainfall intensities (4–6 mm h^{-1}, Fig. 3a), the MP-*DSD* substantially overestimates the proportion of small drops (< 0.25 mm), but underestimates the amount of all other drop size classes. (ii) For moderate rainfall intensities (20–30 mm h^{-1}) the MP distribution predicts the proportion of the smallest drops size class and furthermore large drops appropriately (> 1 mm, Fig. 3b). (iii) However, the proportions of large drops are systematically overestimated by the MP distribution for high intensities (40–60 and 100–150 mm h^{-1}, Fig. 3c and d).

Comparing measured drop fall velocities against the theoretical fall

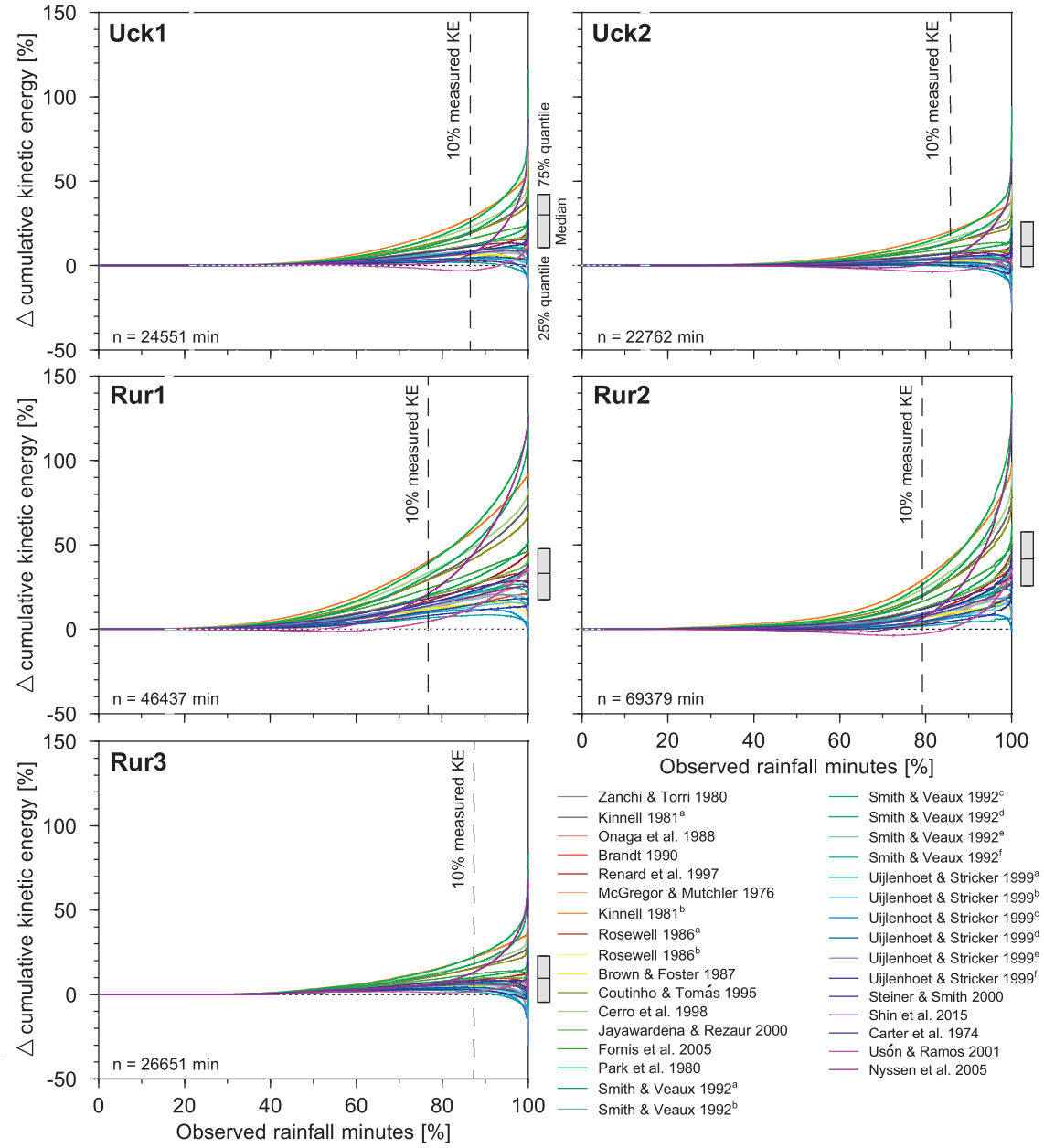

Fig. 5. Cumulative deviation, increasingly sorted according to measured kinetic energy (*KE*), between measured and derived *KE* by 32 different rainfall kinetic energy-intensity relations (see Table 1). Vertical dashed line shows 10% of cumulative measured *KE* sum. (For interpretation of the references to colour in this figure legend, the reader is referred to the web version of this article.)

velocity model of Gunn and Kinzer (1949; GK), exemplarily shown for two events of station Uck1, also indicates pronounced deviations (Fig. 4). Particularly for the highly erosive rainfall event (Fig. 4a), small drops were measured at almost all fall velocities, where for the low erosive rainfall event (Fig. 4b) the range of measured fall velocity is somewhat smaller. A large proportion of small measured drops show higher fall velocities than predicted by the terminal velocity model by GK. For larger drops, the GK distribution describes more or less the measured fall velocities, but a substantial number of large drops show smaller fall velocities. As these large drops are highly relevant for the *KE*, assuming the GK model leads to an overestimation of *KE* under these conditions. The comparison of measured and theoretical drop size and fall velocity distributions indicates that both potentially lead to *KE* overestimations for large drops.

3.2. Comparison of measured vs. derived kinetic energy

We analysed the deviation between measured and derived *KE* by 32 *KE-I* relations. The majority of *KE-I* relations show an overestimation of cumulative *KE* with a large variety of results (Fig. 5). The deviation was not uniformly distributed throughout the course of increasing measured *KE*. In general, there are mainly three kinds of behaviour of the *KE-I* relations: (i) an exponentially increasing overestimation, (ii) a pronounced underestimation of the strongest 10% of rainfall minutes. (iii) A number of relations do show a conservative behaviour and lead to a constant overestimation (without exponential deviation at high energies) throughout the course of different energy levels (Fig. 5). The minutes of highest *KE* are proportionally more relevant for the total *KE* of the data series at the Uckermark stations compared to the Rur stations (Fig. 5). Hence, 90% of the total *KE* was achieved by 13.5% and 14.7% of rainfall minutes for Uck1 and Uck2, respectively (Rur1:

Table 3
Annual deviation of 32 kinetic energy-intensity relations to measured kinetic energy over 5 stations and a total of 13 yrs (see Table 2). Relative deviation (%) is given in brackets behind absolute deviation (J m^{-2}). Positive values indicate an overestimation and negative values an underestimation of the measured kinetic energy.

Station	Year	Measured *KE*	Δ measured *KE*	
		[J m^{-2}]	Mean	Median
Uck1	2015	2152	788 (36.6)	635 (29.5)
	2016	3203	870 (27.2)	700 (21.9)
Uck2	2015	3173	462 (10.9)	273 (8.7)
	2016	4247	742 (8.2)	568 (6.5)
Rur1	2015	6278	3036 (48.4)	2531 (40.3)
	2016	5519	1845 (33.4)	1416 (25.7)
Rur2	2013	4236	1810 (42.7)	1370 (32.3)
	2015	4444	3134 (70.5)	2738 (61.6)
	2016	3133	963 (30.7)	883 (28.2)
Rur3	2013	5846	283 (4.8)	−11 (−0.2)
	2014	1604	906 (56.5)	790 (49.2)
	2015	2106	22 (1.0)	−66 (−3.1)

23.3%, Rur2: 20.8%). In contrast, the largest contribution of heavy precipitation minutes was found for station Rur3 (12.6%).

On an annual aggregation level, all years at all stations show a mean overestimation of the 32 *KE-I* relations compared to the measured *KE* (Table 3). The highest annual deviations are found for the stations Rur1 and Rur2, which are located in the hilly Eifel region. The highest mean deviation of 71% for a measured total annual *KE* sum of 4.4 kJ m^{-2} was found at station Rur2 in 2015. The lowest annual deviation was shown for station Rur3 with a relative mean deviation of 1% for a total *KE* sum of 2106 J m^{-2}.

3.3. Measured vs. derived kinetic energy affecting event erosivity

Analysing event differences for measured and derived *KE* in relation to erosivity, shows distinct differences between the Uckermark and Rur stations. Uck1 and Uck2 are dominated by events with low rainfall erosivities < 5 N h^{-1}, while the Rur stations show regularly occurring events of higher rainfall erosivities between 5 and 20 N h^{-1} (Fig. 6; Table 2). Events of long duration (> 2.5 days) can accumulate large quantities of *KE* but do not have high rainfall intensities and therefore low erosivities. A long duration event at Rur1 (approx. 10 N h^{-1}; Fig. 6b) shows the largest 95% confidence interval for the 32 *KE-I* relations, ranging from 1.3 to 3 kJ m^{-2}. Surprisingly, this large range does not cover the measured *KE* (1.2 kJ m^{-2}; Fig. 6). As already shown by the analysis of minute-wise data, the derived *KE* distinctively overestimates the measurements, which is indicated by the median PBIAS (average over- or underestimation between derived and measured *KE* values in percent) of all *KE-I* relations, ranging from 10 to 54%. *KE-I* relations originally developed for Spain (Usón and Ramos, 2001) and North Carolina (Smith and De Veaux, 1992) matched the events of the Uckermark stations best, where *KE-I* relations theoretically developed from *DSDs* (Uijlenhoet and Stricker, 1999) performed best for Rur1 and Rur2. The heavy event at the stations Uck1 and Uck2 in 2016 (Fig. 6a) contributes only with 11% and 17% to the total *KE* but with 46% and 60% of the total rainfall erosivity, respectively. Although single events have limited impact on the total *KE* sum of a time series, the relevance of single events for the total rainfall erosivity is high. Noteworthy, the Uckermark stations are located 300 m apart, but show substantial differences (Table 3).

3.4. Modelled differences in sediment delivery

Appling the WaTEM/SEDEM model with altered *R* and *C* factors in relation to different rainfall *KE-I* relations shows high variations in sediment delivery (Fig. 7). Where the reference runs (based on measured

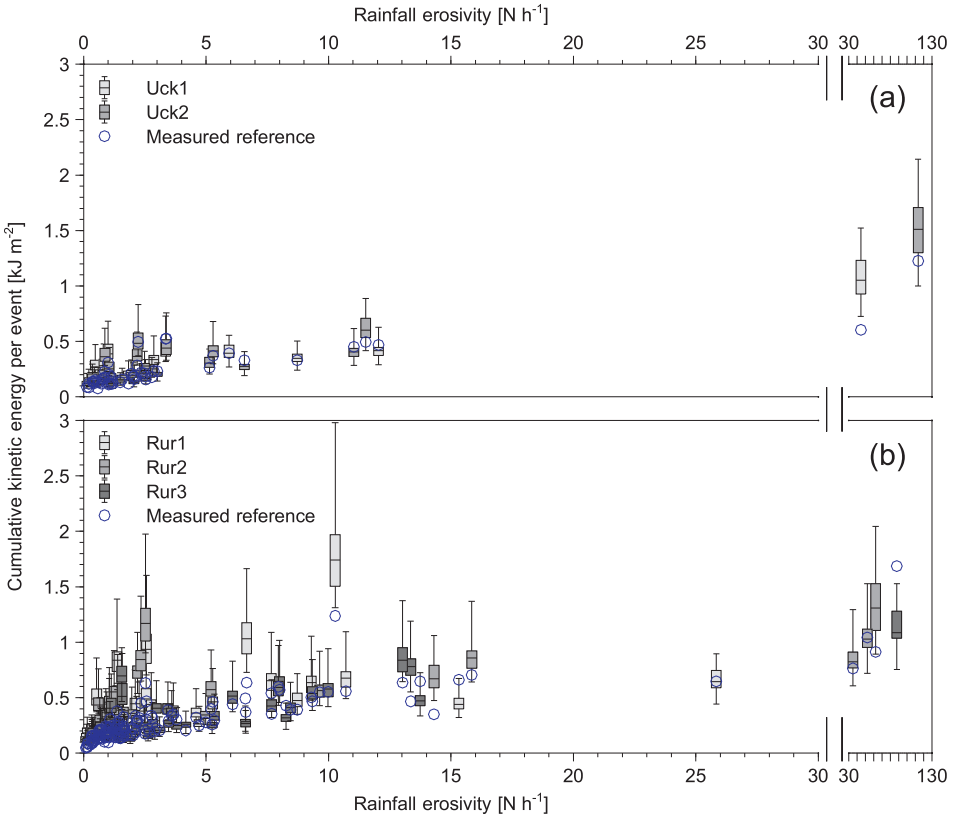

Fig. 6. Event based kinetic energy derived by 32 different kinetic energy-intensity relations (box-whiskers). Error bars indicate the 95% interval of confidence. The blue circles show the measured kinetic energy. (For interpretation of the references to colour in this figure legend, the reader is referred to the web version of this article.)

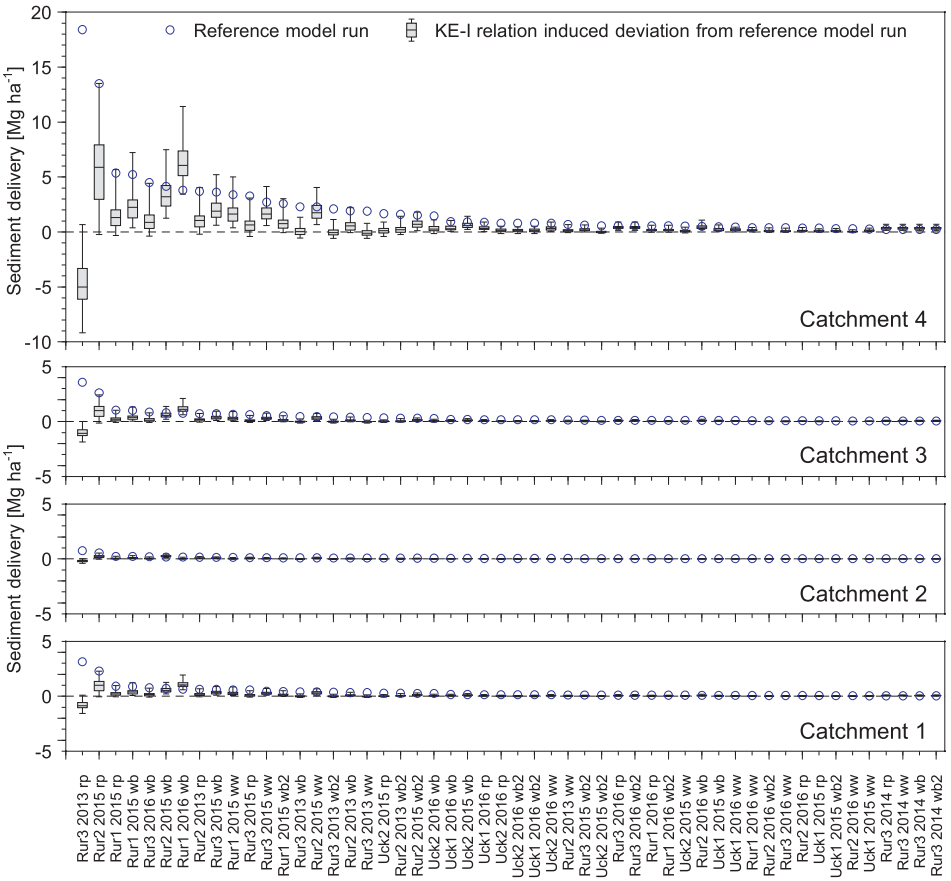

Fig. 7. Modelled (WaTEM/SEDEM) uncertainty in annual sediment delivery related to 32 different theoretical rainfall kinetic energy-intensity (*KE-I*) relations (see Table 1), altering the *R* (rainfall erosivity) and *C* (management) factor of the RUSLE. The blue circles indicate the modelled absolute sediment delivery (sorted in descending order according to the reference model runs), whereas the boxes (25 and 75%) and whiskers (5 and 95%) show the deviation between the reference model run and the *KE-I* relation model runs. The model applies 13 yrs. of rainfall data of 5 station to a complete crop rotation in four catchments (see Fig. 2; rp: rape, ww: winter wheat, wb: winter barley, wb2: winter barley second year). (For interpretation of the references to colour in this figure legend, the reader is referred to the web version of this article.)

rainfall *KE*), show for the larger catchments (C1 to C3; Fig. 2) moderate sediment delivery ($< 4\,\mathrm{Mg\,ha^{-1}\,yr^{-1}}$), the highly connected catchment 4 shows annual sediment delivery up to $18\,\mathrm{Mg\,ha^{-1}\,yr^{-1}}$. Catchment 2, which is the largest catchment that consists of erosional and depositional structures (Fig. 8), shows the lowest reaction on different *KE-I* relations. Contrary to that, the smallest and mainly erosion dominated catchment 4 shows the largest sediment delivery feedback in response to alterations in the derived *KE* from 13 up to $27\,\mathrm{Mg\,ha^{-1}\,yr^{-1}}$. Interestingly, the model runs of highest sediment delivery show conflicting results in relation to the corresponding reference runs. The year of highest sediment delivery (Rur3, 2013) shows a median underestimation of $5\,\mathrm{Mg\,ha^{-1}\,yr^{-1}}$, where the second highest year (Rur2, 2015) has a median overestimation of $5.9\,\mathrm{Mg\,ha^{-1}\,yr^{-1}}$ in catchment 4. Substantial sediment delivery was solely simulated for rainfall data of the Rur stations (Fig. 7). The extreme event at the Uckermark stations in 2016 occurred in times of high soil cover and does not cause substantial simulated sediment delivery. Highest sediment delivery of the crop rotation is caused by rape cultivation.

4. Discussion

Optical distrometers have potential error sources e.g. splash from device arm into the sensor, two drops detected as a single drop, horizontal moving drops by wind (Angulo-Martinez et al., 2016). Nonetheless, optical distrometers enable the continuous observation of rainfall *KE* dynamics on high temporal resolution. Due to dynamics in drop size distributions (*DSD*) according to the type of rainfall, the *KE-I* relationship is not static for different events and furthermore throughout different event phases (Angulo-Martinez et al., 2016). However, almost all *KE-I* relations are explicitly developed for one typical *DSD* of a single distinct meteorological region, rainfall type and utilize static drop size specific fall velocities. Therefore, combined measurements of *DSD* and corresponding fall velocities by optical distrometers are assumed to be the most accurate and available source to measure and analyze rainfall *KE* dynamics.

4.1. High resolution analysis

The minute based analysis shows pronounced deviations between measured and derived *KE* (Fig. 5), which is in line with earlier studies (e.g. Angulo-Martinez et al., 2016; Petan et al., 2010; Salles et al., 2002). Specific deviations in reaction to different rainfall *KE-I* relations are shown. A few *KE-I* relations match the total sum of measured *KE* after the complete time series well, but nonetheless do have a large absolute error, caused by high deviations over the course of different *KE* levels. The majority of *KE-I* relations show a distinct overestimation (Fig. 5), which is likely to be caused by a large number of drops falling at velocities conflicting common models of terminal velocity (Gunn and Kinzer, 1949; Hinkle et al., 1987; Laws, 1941) used to derive theoretical *KE-I* relations. We observed a large quantity of small drops (< 0.75 mm) falling at extraordinarily high velocities (Fig. 4). These super-terminal drops are reported in literature and are likely to be caused by wind effects (Montero-Martinez and Garcia-Garcia, 2016) and fragmentation of fast and large drops (Larsen et al., 2014). Since super-terminal drops have higher energies than estimated from theoretical terminal velocity models, they cause an underestimation of *KE-I* relations. However, Fig. 4 shows that the amount of *KE* caused by drops smaller than 0.75 mm is rather limited for the overall *KE* estimation. Furthermore, we observed drops falling at substantially lower velocities than expected from terminal velocity models (Fig. 4), which were also observed in other studies (Angulo-Martinez et al., 2016; Cerro et al., 1998; Montero-Martinez and Garcia-Garcia, 2016; Petan et al., 2010). Sub-terminal drops cause an overestimation for *KE-I* relationships and mainly occur in the drop diameter class contributing to the highest

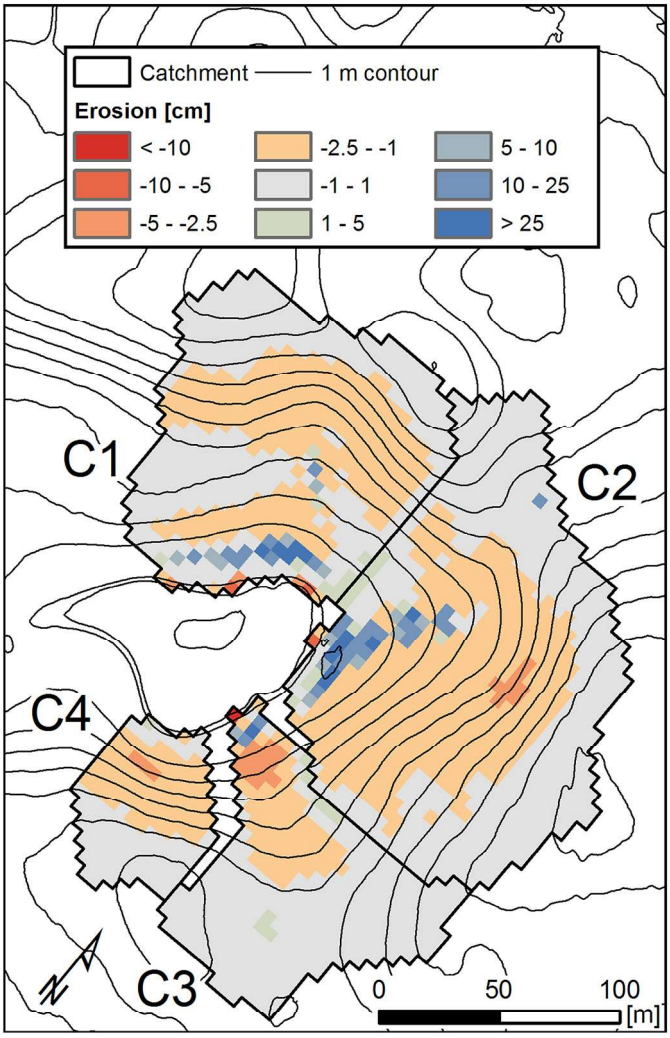

Fig. 8. Cumulative soil erosion (negative values) and deposition (positive values) by water of all 52 reference model runs based on measured rainfall kinetic energy. (For interpretation of the references to colour in this figure legend, the reader is referred to the web version of this article.)

amount of rainfall *KE* (Fig. 4). Therefore, sub-terminal drops and the overestimation of large drops in case of high rainfall intensities (Fig. 3) are likely to be the reason for the disagreement between measured and theoretically derived *KE*. This general overestimation of *KE-I* relations is in line with recently published results of Angulo-Martinez et al. (2016). With similar methodology, they reported a minute based positive bias for the *KE-I* relations compared to optical distrometer based measured *KE*.

4.2. Regional conditions for event based model input

The most common use of *KE-I* relations in soil erosion modelling, is to provide region-specific event based kinetic energies. Interestingly, the best matching *KE-I* relations are not necessarily developed for similar regions or environmental conditions. One could argue that the good performance for Uck1 and Uck2 of the *KE-I* relation developed for Spain (Usón and Ramos, 2001) is attributed to meteorological similarities, such as convective rainfall of high intensities. However, Usón and Ramos (2001) developed this relation based on data with a maximum rainfall intensity of 20 mm h^{-1}. Since our rainfall records consist of measurements of much higher rainfall intensities (up to 300 mm h^{-1}), the good agreement cannot be attributed to meteorological reasons due to heavy uncertainties by extrapolation.

We found regional differences in estimate quality. The predictions for the Uckermark stations were better compared to the Rur stations, which is potentially caused by less variation in rainfall types. In contrast to the predominantly cyclonic rainfall in the maritime climate of the Rur stations, the short and heavy convective rainfall in the subcontinental climate of the Uckermark might have less variation in *DSD*, which leads to a better predictability of static *KE-I* relations. Furthermore, the stations Rur1 and Rur2 are located in the hilly Eifel region that may cause larger dynamics in rainfall types and corresponding *DSD*, which may to some extent explain the poor estimate quality at these two particular stations (Tables 3 and 4). Therefore, it is suggested to select the utilized *KE-I* relation on event level in relation to the rainfall type or seasonal rainfall patterns and not only for a distinct meteorological region.

4.3. Soil erosion modelling

The parsimonious WaTEM/SEDEM model showed its reliability in predicting soil erosion estimates in numerous studies for different environments (e.g. Bakker et al., 2008; De Vente et al., 2008; Dlugoß et al., 2012; Nadeu et al., 2015; Van Rompaey et al., 2005; Verstraeten et al., 2002). Due to the virtual input data, a rigorous validation was not possible. However, with respect to the study aim of quantifying the range of possible uncertainties induced by a variety of *KE-I* relations and focusing on relative differences, the model performance is assumed to be sufficiently good.

Sediment delivery is substantially affected by the seasonal distribution of rainfall *KE* occurrence. For the year of the highest *KE* and *R* factor, low sediment delivery was simulated because the largest energy proportion occurred during a period of full vegetation cover. Thus, pronounced sediment delivery was solely simulated for the rainfall data of the cyclonic Rur stations due to a higher event frequency. An altered seasonal rainfall distribution would cause much higher sediment delivery and thus our estimates are rather conservative. Soil erosion by water is a highly episodic process, driven by single events (Fiener et al., 2015; Wilken et al., 2017) and requires a combination of environmental conditions. Unfortunately, extreme events show the highest variation and uncertainty of the *KE-I* relationship. Fig. 7 illustrates that the deviation is not constant throughout all years of highest sediment delivery and can either over or underestimate the reference run considerably. This implies for water erosion modelling, that *KE* derived from rainfall intensity underlies large uncertainties for rare and highly important extreme events. This might be particularly true for physically-oriented models that apply *KE-I* relations on high temporal resolution. In contrast, on long time scales, the error might to some extent average out when utilizing conceptual models that were originally developed for the prediction of long-term average soil loss such as the USLE (Wischmeier and Smith, 1960).

The majority of environmental studies utilize tipping bucket rain gauges, which have a known underestimation problem of high intensity rainfall (Humphrey et al., 1997; Marsalek, 1981; Shedekar et al., 2016). Since most *KE-I* relations were developed to be applied on tipping bucket rain gauges, the positive bias might intentionally compensate the mechanically caused underestimation. Petan et al. (2010) showed that the derived *KE* from tipping bucket rain gauges is distinctively lower compared to the measured *KE* based on two optical laser distrometers (Thies-Clima and OTT). However, this would suggest that traditional *KE-I* relations need to be calibrated for an application on intensity measurements of modern ombrometers.

5. Conclusions

We applied various rainfall kinetic energy-intensity (*KE-I*) relations on five optical distrometers to assess (i) deviations between measured and theoretically derived kinetic energy (*KE*), (ii) variations throughout different energy and temporal aggregation levels and (iii) implications

for soil erosion modelling. Pronounced differences between measured and modelled (Gunn and Kinzer, 1949; Marshall and Palmer, 1948) drop size and fall velocity distributions were found, which cause a substantial overestimation of *KE-I* relations compared to measured *KE* Meteorological regions of highly complex rainfall regimes show larger differences between measured and derived *KE* compared to locations of a single dominant rainfall type. Hence, the geographical region is not necessarily the best predictor to determine the most adapted *KE-I* relation for a study area with heterogeneous rainfall characteristics. Our results highlight large uncertainties far from negligible for soil erosion modelling that are associated to theoretical *KE-I* relations (range in sediment delivery from 10 to 27 t ha^{-1}).

Acknowledgements

The study was supported by the Terrestrial Environmental Observatory TERENO-Northeast of the Helmholtz Association. The optical distrometer measurements were carried out in the framework of the Helmholtz-funded TERENO (http://teodoor.icg.kfa-juelich.de/overview-de) project. We gratefully acknowledge the careful maintenance of stations Uck1 and Uck2 by Peter Rakowski. Ferdinand Engels and Alexander Graf kindly provided the data of the stations Rur1 to Rur3. Special thanks also go to the farm owner Bernd Sohn for his permission to carry out various types of measurements on his field in the Uckermark.

References

Aldana-Jague, E., Sommer, M., Saby, N.P.A., Cornelis, J.T., Van Wesemael, B., Van Oost, K., 2016. High resolution characterization of the soil organic carbon depth profile in a soil landscape affected by erosion. Soil Tillage Res. 156, 185–193.

Angulo-Martinez, M., Begueria, S., Kysely, J., 2016. Use of disdrometer data to evaluate the relationship of rainfall kinetic energy and intensity (KE-I). Sci. Total Environ. 568, 83–94.

Bakker, M.M., Govers, G., Van Doorn, A., Quetier, F., Chouvardas, D., Rounsevell, M., 2008. The response of soil erosion and sediment export to land-use change in four areas of Europe: the importance of landscape pattern. Geomorphology 98, 213–226.

Bentley, W., 1904. Studies of raindrops and raindrop phenomena. Mon. Weather Rev. (10), 450–456.

BGR, 2014. Erodierbarkeit der Ackerböden durch Wasser in Deutschland. (Bundesanstalt für Geowissenschaften und Rohstoffe).

Cerro, C., Bech, J., Cordina, B., Lorente, J., 1998. Modeling rain erosivity using disdrometric techniques. Soil Sci. Soc. Am. J. 62, 731–735.

De Roo, A.P., Wesseling, C.G., Ritsema, C.J., 1996. LISEM: a single-event physically based hydrological and soil erosion model for drainage basins. I: theory, input and output. Hydrol. Process. 10, 1107–1117.

De Vente, J., Poesen, J., Verstraeten, G., Van Rompaey, A., Govers, G., 2008. Spatially distributed modelling of soil eroison and sediment yield at regional scale in Spain. Glob. Planet. Chang. 60, 393–415.

Desmet, P.J.J., Govers, G., 1996. A GIS procedure for automatically calculating the USLE LS factor on topographically complex landscape units. J. Soil Water Conserv. 51, 427–433.

Deumlich, D., 1999. Erosive Niederschläge und ihre Eintrittswahrscheinlichkeit im Norden Deutschlands. Meteorol. Z. 8, 155–161.

Dlugoß, V., Fiener, P., Van Oost, K., Schneider, K., 2012. Model based analysis of lateral and vertical soil C fluxes induced by soil redistribution processes in a small agricultural watershed. Earth Surf. Process. Landf. 37 (2), 193–208.

Fiener, P., Dlugoß, V., Van Oost, K., 2015. Erosion-induced carbon redistribution, burial and mineralisation - is the episodic nature of erosion processes important? Catena 133, 282–292.

Gerke, H.H., Hierold, W., 2012. Vertical bulk density distribution in C-horizons from marley till as indicator for erosion history in a hummocky post-glacial soil landscape. Soil Tillage Res. 125, 116–122.

Gerke, H.H., Koszinski, S., Kalettka, T., Sommer, M., 2010. Structures and hydrologic function of soil landscapes with kettle holes using an integrated hydropedological approach. J. Hydrol. 393 (1–2), 123–132.

Graf, A., Bogena, H.R., Drue, C., Hardelauf, H., Putz, T., Heinemann, G., Vereecken, H., 2014. Spatiotemporal relations between water budget components and soil water content in a forested tributary catchment. Water Resour. Res. 50 (6), 4837–4857.

Gunn, R., Kinzer, D., 1949. The terminal velocity of fall for water droplets in stagnant air. J. Meteorol. 6, 243–248.

Hinkle, S.E., Heermann, D.F., Blue, M.C., 1987. Falling water drop velocities at 1570 m (5150 ft) elevation. Trans. ASAE 30 (1), 15.

Humphrey, M.D., Istok, J.D., Lee, J.Y., Hevesi, J.A., Flint, A.L., 1997. A new method for automated dynamic calibration of tipping-bucket rain gauges. J. Atmos. Ocean. Technol. 14 (6), 1513–1519.

IUSS, 2015. World reference base for soil resources 2014. Update 2015. International soil classification system for naming soils and creating legends for soil maps. In: World Soil Resources Reports No. 106. FAO, Rome.

Kinnell, P.I.A., 2005. Raindrop-impact-induced erosion processes and prediction: a review. Hydrol. Process. 19 (14), 2815–2844.

Larsen, M.L., Kostinski, A.B., Jameson, A.R., 2014. Further evidence for superterminal raindrops. Geophys. Res. Lett. 41 (19), 6914–6918.

Laws, J.O., 1941. Measurements of the fall-velocity of water-drops and raindrops. Trans. Am. Geophys. Union 22, 709–721.

Laws, J.O., Parsons, D.A., 1943. The relation of raindrop-size to intensity. Trans. Am. Geophys. Union 24, 452–459.

Lim, Y.S., Kim, J.K., Kim, J.W., Park, B.I., Kim, M.S., 2015. Analysis of the relationship between the kinetic energy and intensity of rainfall in Daejeon, Korea. Quat. Int. 384, 107–117.

Marsalek, J., 1981. Calibration of the tipping-bucket raingage. J. Hydrol. 53 (3–4), 343–354.

Marshall, J.S., Palmer, W.M., 1948. The distribution of raindrops with size. J. Meteorol. 5 (4), 165–166.

McCool, D.K., Brown, L.C., Foster, G.R., Mutchler, C.K., Meyer, L.D., 1987. Revised slope steepness factor for the universal soil loss equation. Trans. ASAE 30, 1387–1396.

Montero-Martinez, G., Garcia-Garcia, F., 2016. On the behaviour of raindrop fall speed due to wind. Q. J. R. Meteorol. Soc. 142 (698), 2013–2020.

Morgan, R.P.C., 2005. Soil Erosion and Conservation, 3. Blackwell Publishing, Oxford, pp. 304.

Morgan, R.P.C., Quinton, J.N., Smith, R.E., Govers, G., Poesen, J.W.A., Auerswald, K., Chisci, G., Torri, D., Styczen, M.E., 1998. The European soil erosion model (EUROSEM): a dynamic approach for predicting sediment transport from fields and small catchments. Earth Surf. Process. Landf. 23, 527–544.

Nadeu, E., Gobin, A., Fiener, P., Van Wesemael, B., Van Oost, K., 2015. Modelling the impact of agricultural management on soil carbon stocks at the regional scale: the role of lateral fluxes. Glob. Chang. Biol. 21 (8), 3181–3192.

Petan, S., Rusjan, S., Vidmar, A., Mikos, M., 2010. The rainfall kinetic energy-intensity relationship for rainfall erosivity estimation in the Mediterranean part of Slovenia. J. Hydrol. 391 (3–4), 314–321.

Puetz, T., Kiese, R., Wollschlager, U., Groh, J., Rupp, H., Zacharias, S., Priesack, E., Gerke, H.H., Gasche, R., Bens, O., Borg, E., Baessler, C., Kaiser, K., Herbrich, M., Munch, J.C., Sommer, M., Vogel, H.J., Vanderborght, J., Vereecken, H., 2016. TERENO-SOILCan: a lysimeter-network in Germany observing soil processes and plant diversity influenced by climate change. Environ. Earth Sci. 75 (18).

Reichenau, T.G., Korres, W., Montzka, C., Fiener, P., Wilken, F., Stadler, A., Waldhoff, G., Schneider, K., 2016. Spatial heterogeneity of leaf area index (LAI) and its temporal course on arable land: combining field measurements, remote sensing and simulation in a comprehensive data analysis approach (CDAA). PLoS One 11 (7).

Renard, K.G., Foster, G.R., Weesies, G.A., McCool, D.K., Yoder, D.C., 1996. Predicting soil erosion by water: A guide to conservation planning with the Revised Universal Soil Loss Equation (RUSLE). In: Agricultural Handbook 703. USDA-ARS, Washington DC.

Renard, K.G., McCool, D.K., Cooley, K.R., Foster, G.R., Istok, J.D., Mutchler, C.K., 1997. Rainfall-runoff erosivity factor (R). In: Renard, K.G., Foster, G.R., Weesies, G.A., McCool, D.K., Yoder, D.C. (Eds.), Predicting soil erosion by water: A guide to conservation planning with the revised universal soil loss equation (RUSLE). Agric. Handb. No. 703. U.S. Gov. Print Office, Washington D.C., pp. 19–64.

Salles, C., Poesen, J., Sempere-Torres, D., 2002. Kinetic energy of rain and its functional relationship with intensity. J. Hydrol. 257 (1–4), 256–270.

Sanchez-Moreno, J.F., Mannaerts, C.M., Jetten, V., Loffler-Mang, M., 2012. Rainfall kinetic energy-intensity and rainfall momentum-intensity relationships for Cape Verde. J. Hydrol. 454, 131–140.

Schwertmann, U., Vogl, W., Kainz, M., 1990. Bodenerosion durch Wasser - Vorhersage des Abtrags und Bewertung von Gegenmaßnahmen, 2. Ulmer Verlag, Stuttgart (64 pp).

Sempere-Torres, D., Sanchez-Diezma, R., Zawadzki, I., Creutin, J.D., 2000. Identification of stratiform and convective areas using radar data with application to the improvement of DSD analysis and Z-R relations. Phys. Chem. Earth Part B 25 (10—12), 985–990.

Shedekar, V.S., King, K.W., Fausey, N.R., Soboyejo, A.B.O., Harmel, R.D., Brown, L.C., 2016. Assessment of measurement errors and dynamic calibration methods for three different tipping bucket rain gauges. Atmos. Res. 178, 445–458.

Smith, J.A., De Veaux, R.D., 1992. The temporal and spatial variability of rainfall power. Environmetrics 3 (1), 29–53.

Sommer, M., Gerke, H.H., Deumlich, D., 2008. Modelling soil landscape genesis — a "time split" approach for hummocky agricultural landscapes. Geoderma 145 (3–4), 480–493.

Thies-Clima, 2011. Laser Precipitation Monitor - Instructions for Use. Thies-Clima, Göttingen.

Uijlenhoet, R., Stricker, J.N.M., 1999. Dependence of rainfall interception on drop size - a comment. J. Hydrol. 217 (1–2), 157–163.

Usón, A., Ramos, M.C., 2001. An improved rainfall erosivity index obtained from experimental interrill soil losses in soils with a Mediterranean climate. Catena 43 (4), 293–305.

Van Oost, K., Govers, G., Desmet, P., 2000. Evaluating the effects of changes in landscape structure on soil erosion by water and tillage. Landsc. Ecol. 15, 577–589.

Van Oost, K., Govers, G., Van Muysen, W., 2003. A process-based conversion model for caesium-137 derived erosion rates on agricultural land: an integrated spatial approach. Earth Surf. Process. Landf. 28 (2), 187–207.

Van Oost, K., Quine, T., Govers, G., Heckrath, G., 2005. Modeling Soil Erosion Induced Carbon Fluxes between Soil and Atmosphere on Agricultural Land Using SPEROS-C. In: Roose, E.J., Lal, R., Feller, C., Barthes, B., Stewart, B.A. (Eds.), Advances in Soil Science. Soil Erosion and Carbon Dynamics. CRC Press, Boca Raton, pp. 37–51.

Van Rompaey, A.J.J., Verstraeten, G., Van Oost, K., Govers, G., Poesen, J., 2001.

Modelling mean annual sediment yield using a distributed approach. Earth Surf. Process. Landf. 26 (11), 1221–1236.
Van Rompaey, A., Bazzoffi, P., Jones, R.J.A., Montanarella, L., 2005. Modeling sediment yields in Italian catchments. Geomorphology 65 (1–2), 157–169.
Verstraeten, G., Van Oost, K., Van Rompaey, A., Poesen, J., Govers, G., 2002. Evaluating an integrated approach to catchment management to reduce soil loss and sediment pollution through modelling. Soil Use Manag. 19, 386–394.
Verstraeten, G., Poesen, J., Gillijns, K., Govers, G., 2006. The use of riparian vegetated filter strips to reduce river sediment loads: an overestimated control measure? Hydrol. Process. 20 (20), 4259–4267.
Vogel, E., Deumlich, D., Kaupenjohann, M., 2016. Bioenergy maize and soil erosion - risk assessment and erosion control concepts. Geoderma 261, 80–92.
Wiesner, J., 1895. Beiträge zur Kenntnis des tropischen Regens. In: Sitzungsber. Akad. Wiss. Wien. 104. pp. 1397–1434.
Wilken, F., Fiener, P., Van Oost, K., 2017. Modelling a century of soil redistribution processes and carbon delivery from small watersheds using a multi-class sediment transport model. Earth Surf. Dyn. 5 (1), 113–124.
Wischmeier, W.H., Smith, D.D., 1958. Rainfall energy and its relationship to soil loss. Trans. Am. Geophys. Union 39, 285–291.
Wischmeier, W.H., Smith, D.D., 1960. A universal soil-loss equation to guide conservation farm planning. In: Trans. Int. Congr. Soil Sci., 7th, pp. 418–425.
Zacharias, S., Bogena, H., Samaniego, L., Mauder, M., Fuss, R., Putz, T., Frenzel, M., Schwank, M., Baessler, C., Butterbach-Bahl, K., Bens, O., Borg, E., Brauer, A., Dietrich, P., Hajnsek, I., Helle, G., Kiese, R., Kunstmann, H., Klotz, S., Munch, J.C., Papen, H., Priesack, E., Schmid, H.P., Steinbrecher, R., Rosenbaum, U., Teutsch, G., Vereecken, H., 2011. A network of terrestrial environmental observatories in Germany. Vadose Zone J. 10 (3), 955–973.